Macro- and Micro-mechanical Responses of Granular Materials Under Different Stress Paths Using DEM

M. M. Sazzad, M. S. Azad, and A. Ghosh

1 Introduction

Stress path is very important in geotechnical engineering which represents the successive states of stress in granular materials such as sand during loading or unloading while carrying out the laboratory tests on test specimens. Due to the variation of the stress states, granular materials also respond differently. The study of stress paths is important for formulating different constitute equations. The stress paths usually studied in geotechnical engineering include conventional triaxial compression, triaxial compression, axial extension, plane strain compression, mean stress compression, reduced triaxial compression, reduced triaxial extension, and hydrostatic compression. Being a very important part of geotechnical engineering studies, numerous experimental studies were carried out and reported in the literature considering stress paths [1–3]. The experimental results are then used to develop constitutive equations to predict the complex behavior of granular materials under different loading conditions. Since the constitutive modeling of granular materials under different loading conditions mainly depends on the boundary behavior obtained from the laboratory tests without considering the inherent particulate behavior, the geotechnical engineers often rely on the experiences and judgments. To develop a constitutive model based on the inherent micro-mechanics, the evolution of the microstructures and their characteristics must be incorporated into the constitutive

M. M. Sazzad (✉)
Department of Civil Engineering, Rajshahi University of Engineering & Technology, Rajshahi, Bangladesh

M. S. Azad
Department of Civil and Environmental Engineering, Konkuk University, Seoul, Republic of Korea
e-mail: samdaniazad@konkuk.ac.kr

A. Ghosh
Department of Civil Engineering, Port City International University, Chittagong, Bangladesh

© The Author(s), under exclusive license to Springer Nature Singapore Pte Ltd. 2022

S. Arthur et al. (eds.), *Advances in Civil Engineering*, Lecture Notes in Civil Engineering 184, https://doi.org/10.1007/978-981-16-5547-0_9

laws. Few studies in the literature have attempted to understand the complex inherent microstructures that evolve under complex loading conditions. Among others, Ng [4] studied six different stress paths and indicated that simulated behavior is very similar to the laboratory results under different loading conditions for sands. It was also reported that the difference between the triaxial compression and plane strain compression is very similar to that observed for sands. A comparison between the conventional triaxial compression and plane strain compression was also reported by Sazzad and Suzuki [5], and a strong correlation between the evolution of the stress–strain and the fabric ratio–strain was established under these loading conditions. Their study observed a unique macro–micro-relationship regardless of the stress paths and loading conditions. Similar other studies in the literatures [6–11] reported the influence of stress paths on the macro-scale (behavior at the boundary) and the micro-scale (behavior at the particle level). In this paper, a comprehensive study is attempted to explore both the macro- and micro-mechanical behaviors of granular materials under four different stress paths namely triaxial compression, plane strain compression, axial extension, and mean stress compression. To carry out the simulation, a numerical sample consisting of spheres was prepared. In this study, spheres were used to reduce the computational costs of the simulation. The isotropically compressed sample was subjected to four different stress paths. Same isotropically compressed sample was used for each simulation to eliminate the biasness of the initial fabric prior to shear of the sample under different stress paths. The simulated data were investigated comprehensively, and the results were reported.

2 Discrete Element Method

The discrete element method (DEM) is a very popular method nowadays to study the microstructural behavior of a granulate system. It is introduced by Cundall and Strack [12]. It is widely used in different branches of science and engineering particularly in geotechnical engineering [4, 6, 9]. The basic structures and equations involved in DEM are very simple, yet its computer programming is complicated and requires huge time to run. Newton's second law of motion is used to obtain the displacement by double integrations for a very small time step. Force–displacement law is used to compute the force using the incremental displacement. The equations involved are as follows:

$$m\ddot{x}_i = \sum F_i, \quad i = 1 - 3 \tag{1}$$

$$I\ddot{\theta} = \sum M \tag{2}$$

where F_i, M, m, I, $\ddot{x}_i$, and $\ddot{\theta}$ are the force components, moment, mass of particle, moment of inertia, translational acceleration components, and rotational acceleration, respectively.

3 Computer Program

In this study, the computer program OVAL is used [13, 14]. The code is written in FORTRAN language and can run both on Windows and Linux platforms. OVAL was used in many simulations earlier, and its efficacy has been established through several publications [13–17]. A linear contact model is used in the present study. In the linear contact model, three linear springs are used. One linear spring is used in the normal direction, and the others are used in the tangential directions to compute normal and shear forces, respectively. Friction sliders have also been used to facilitate the control of slippage between particles and to incorporate the effect of friction angle. The viscosity coefficients (translation and rotational body damping) in OVAL are a fraction of the critical damping.

4 Sample Generation and Preparation

A numerical sample is generated in a cubical frame. The particles were idealized as spheres to reduce the computational cost of simulation. Consideration of complex particle shapes and a huge number of particles would otherwise require a huge computation time. The spheres were placed in the cube shape sample with the variation of the particle diameters randomly. A representative sample was used, and the number of particles of the representative sample was 8000. The initially generated sample was subjected to isotropic compression step by step by using the periodic boundary, a boundary condition in which a particle that straddled a periodic boundary has a numerical image at the opposite boundary, till the isotropic stress reached 100 kPa. When the isotropic stress reached 100 kPa, the void ratio of the sample became 0.57. It should be noted that the interparticle friction at the stage of the isotropic compression was intentionally turned off to ensure the formation of the densest sample. Later, the desired interparticle friction angle is introduced before the start of the simulation.

5 Simulation Conditions

Simulation of triaxial compression, axial extension, plane strain compression, and mean stress compression was conducted. In the case of the triaxial compression test, the vertical height along x_1—direction decreased with a very small strain increment of 0.00002%, while the stresses in the other two directions (x_2—direction and x_3—direction) remained constant (100 kPa). In the case of the axial extension test, the vertical height along x_1—direction increased with a very small strain increment of 0.00002%, while the stresses in the other two directions (x_2—direction and x_3—direction) remained constant (100 kPa). In the case of the plane strain compression

Table 1 DEM parameters used in the simulations

DEM parameters	Values
Normal contact stiffness, k_n (N/m)	1×10^6
Shear contact stiffness, k_s (N/m)	1×10^6
Mass density (kg/m^3)	2650
Increment of time step (s)	1×10^{-6}
Interparticle friction coefficient (μ)	0–0.50
Damping coefficients	0.05

test, the vertical height along x_1—direction decreased with a very small strain increment of 0.00002%, while the stress in x_3—direction remained constant (100 kPa) and the increment of strain in x_2—remained is zero. In the case of the mean stress compression, the vertical height along x_1—direction decreased with a very small strain increment of 0.00002%, while the mean stress remained constant by adjusting the movement of the other two boundaries along x_2—direction and x_3—direction. The DEM parameters and their corresponding values are presented in Table 1. The simulated conditions are depicted in Fig. 1 as well. It should be noted that the same isotropically compressed sample was used in the simulation, so that no bias of the simulated results was noticed due to the variation of the initial fabric of the sample.

6 Macro-mechanical Behavior

The macro-mechanical behavior is discussed in this section. The relationship between the deviatoric stress and mean stress is depicted in Fig. 2. Here, the deviatoric stress is defined as $q = \sigma_1 - \sigma_3$, and mean stress is defined as $p = (\sigma_1 + \sigma_2 + \sigma_3)/3$, where σ_1, σ_2, and σ_3 are the stresses along x_1, x_2 , and x_3 directions, respectively. Figure 3a depicts the evolution of deviatoric stress with axial strain ε_1. The simulated behavior of the present study is very similar to that observed in the experimental and numerical investigation [4, 5, 10, 11, 18]. The highest deviatoric stress is obtained for plane strain compression (PSC). This is also in accordance with similar other studies in the literature [4, 9]. The deviatoric stress is the minimum for mean stress compression (MSC) as expected. This is due to the continuous rearrangement of the contact fabric during MSC to maintain the target mean stress [4]. Triaxial compression (TC) and axial extension (AE) depict the intermediate behavior where the deviatoric stress in AE is greater than TC [4]. This behavior is consistent with that observed in the sand. The evolution of the volumetric strain defined as $\varepsilon_v = \varepsilon_1 + \varepsilon_2 + \varepsilon_3$ with axial strain ε_1 is depicted in Fig. 3b. The positive sign of ε_v indicates compression, while the negative sign indicates dilation. The compressive behavior is followed by huge dilative behavior regardless of the stress path applied. Such tendency is usual in dense sand. The huge dilation observed in this study particularly in AE is related to the excessive dense soil (void ratio = 0.57) as compared to the other studies in the literature [4, 8, 10].

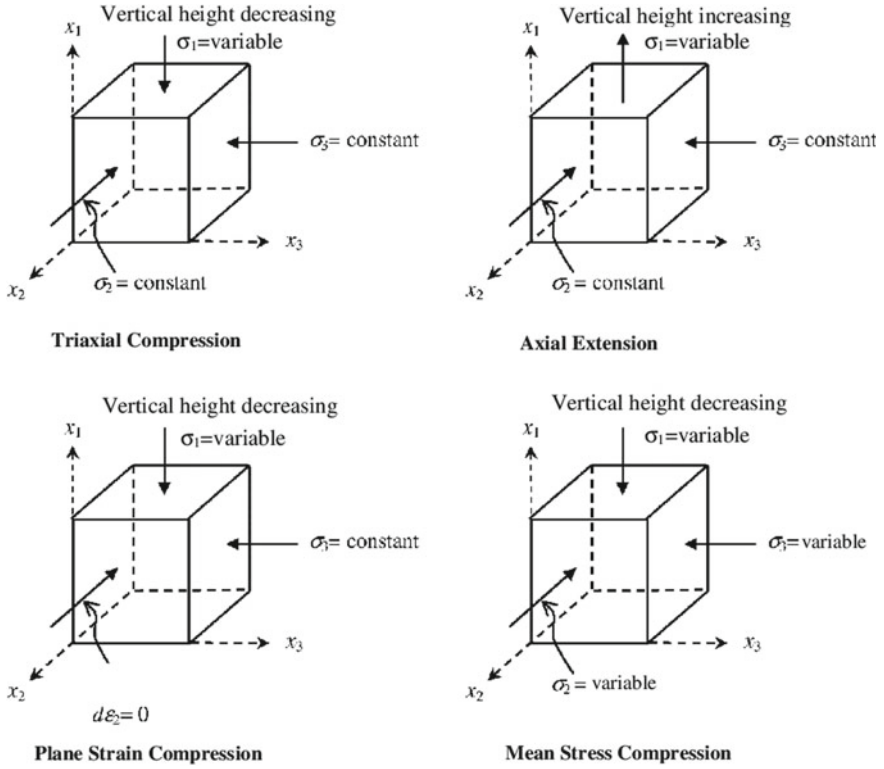

Fig. 1 Graphical representation of the simulation conditions for different stress paths

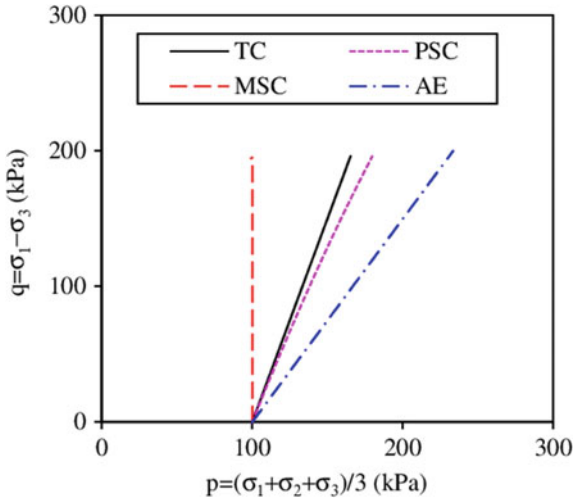

Fig. 2 Relationship between the q and p for different stress paths

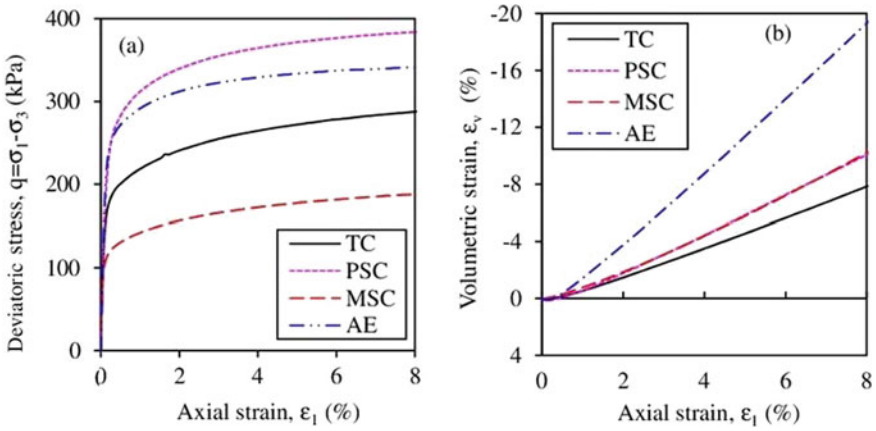

Fig. 3 **a** Relationship between **a** q and ε_1, **b** ε_v and ε_1 for different stress paths

7 Macro-mechanical Behavior

The evolution of different micro-mechanical quantities is discussed in this section. The evolution of the average coordination number defined as twice the total number of contacts divided by the total number of particles considered in the simulation with axial strain is depicted in Fig. 4a. A sharp decrease of average coordination number at the beginning of shear is noticed regardless of the stress path applied. This is because of the disintegration of contacts between particles at the beginning of shear and the fabric of the sample becomes anisotropic from the isotropic state. Although the isotropic condition is the same, a huge loss of average coordination number is

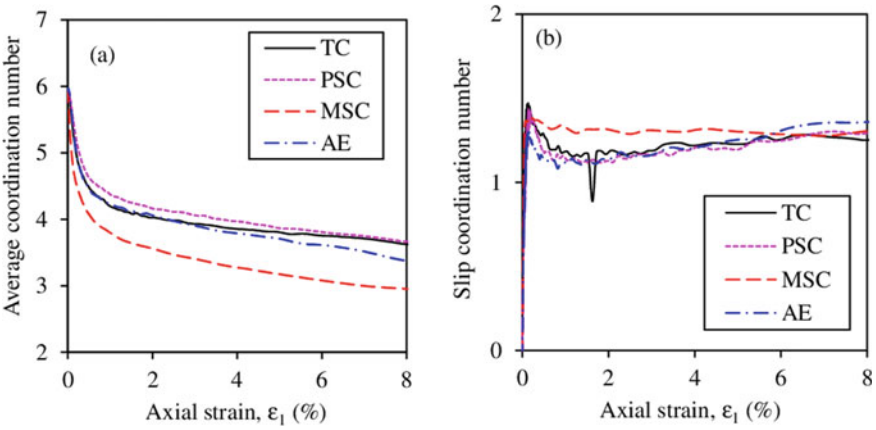

Fig. 4 Evolution of coordination number with axial strain. **a** Average coordination number. **b** Slip coordination number

observed for MSC compared to the other stress paths like TC, PSC, and AE. In the case of MSC, the boundaries of the sample need to move to adjust the target mean stress, and consequently, more contact disintegration takes place resulting in the decrease of average coordination number. On the contrary, the evolution of slip coordination number defined as twice the total number of slip contacts divided by the total number of particles with axial strain is depicted in Fig. 4b. Slip coordination number is sharply picked at a very small strain level, and as the loading continues, it reduces and depicts almost similar behavior regardless of the stress path applied except MSC.

The evolution of deviatoric contact fabric quantified by a fabric tensor considering all and strong contacts between particles is depicted in Fig. 5, while the evolution of contact fabric ratio considering all and strong contacts between particles is depicted in Fig. 6. The fabric tensors considering all and strong contacts are defined as follows [19, 20]:

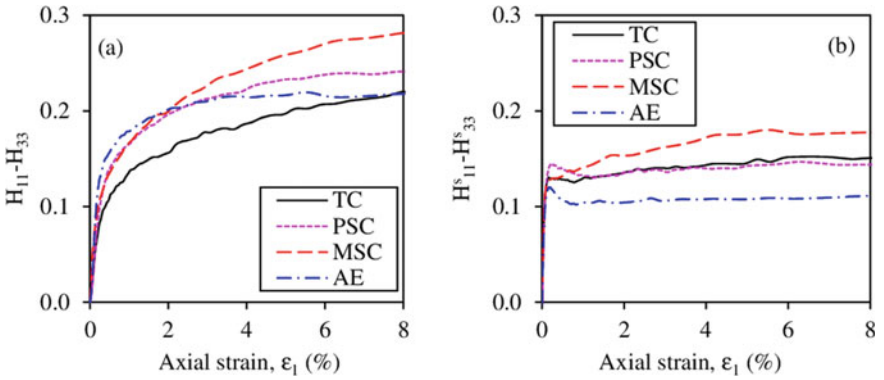

Fig. 5 Evolution of deviatoric contact fabric with axial strain. **a** Considering all contacts. **b** Considering strong contacts only

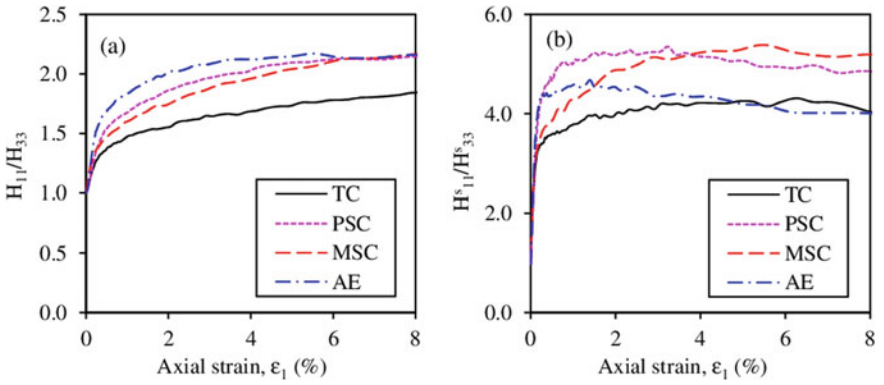

Fig. 6 Evolution of contact fabric ratio with axial strain. **a** Considering all contacts. **b** Considering strong contacts

$$H_{ij} = \frac{1}{N_c} \sum_{c=1}^{N_c} n_i^c n_j^c \qquad i, j = 1 - 3 \tag{3}$$

$$H_{ij}^s = \frac{1}{N_c} \sum_{s=1}^{N_c^s} n_i^s n_j^s \qquad i, j = 1 - 3 \tag{4}$$

Here, n_i^c is the contact normal vector at the i-th contact, and n_i^s is the contact normal vector at the i-th strong contact. N_c and N_c^s are the number of total contacts and number of strong contacts, respectively. A contact is considered to be strong if the normal force between particles during contacts is greater than the average normal force of all contacts. The evolution of deviatoric fabric $H_{11} - H_{33}$ considering all contacts with axial strain is depicted in Fig. 5a, whereas the evolution of deviatoric fabric $H_{11}^s - H_{33}^s$ considering strong contacts with axial strain is depicted in Fig. 5b. A qualitative similarity between the pattern of the evolution of $H_{11} - H_{33}$ with ε_1 and $q = \sigma_1 - \sigma_3$ with ε_1 is noticed. Nevertheless, the quantitative pattern is not similar. For example, q is highest for PSC, whereas $H_{11} - H_{33}$ is highest for MSC. Similar behavior is noticed in Fig. 5b. On the other hand, if the ratio of fabric is considered in contrast to the deviatoric fabric and its evaluation is depicted in Fig. 6, a quantitative similarity between the evolution of stress ratio and fabric ratio with strain is noticed for all other stress paths (TC, PSC, AE) except MSC when strong contacts are considered [compare Fig. 6b with Fig. 3a].

A relationship between fabric ratio considering strong contact and stress ratio is also developed and shown in Fig. 7. A unique behavior is noticed regardless of the stress paths only at a very small strain range (up to 1% of axial strain).

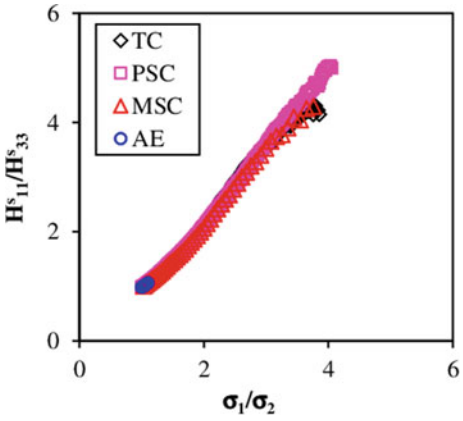

Fig. 7 Relationship between fabric ratio (strong contacts only) and stress ratio for different stress paths

8 Conclusions

A numerical study is conducted using the DEM to explore the micro-mechanical characteristics of a granulate system such as sand for different stress paths. The macro-mechanical behavior is also presented. For this, a numerical sample consisting of 8000 spheres was prepared and compressed isotropically to 100 kPa. The numerical sample was subjected to shear under different stress paths. The same sample prior to shear was used to eliminate the biasness of the initial fabric of the test samples as usually occurred in experimental studies. The simulated macro-mechanical results of the present study were compared with the experimental and numerical results of the earlier published studies and found excellent qualitative agreements among them. Average coordination number and slip coordination number evolve differently with axial strain. A huge loss of average coordination number is observed for mean stress compression compared to other stress paths considered in this study. Slip coordination number sharply picked at a very small strain level and depicts almost similar behavior at the higher strain except mean stress compression. The fabric ratio rather than the deviatoric fabric matches well with the stress ratio rather than the deviatoric stress with strain. The relationship between stress ratio and fabric ratio considering only strong contacts is almost linear and unique regardless of the stress paths only at a very small strain level.

References

1. Tatsuoka F, Sakamoto M, Kawamura F (1986) Strength and deformation characteristics of sand in plane strain compression. Soils Found 26(1):65–84. https://doi.org/org/10.3208/sandf1972.26.65
2. Wang Q, Lade PV (2001) Shear banding in true triaxial tests and its effect on failure in sand. J Eng Mech 127(8):754–761. https://doi.org/org/10.1061/(ASCE)0733-9399(2001)127:8(754)
3. Shapiro S, Yamamuro JA (2003) Effects of silt on three-dimensional stress–strain behavior of loose sand. J Geotech Geoenvir Eng 129(1):1–11. https://doi.org/10.1061/(ASCE)1090-0241(2003)129:1(1)
4. Ng T-T (2005) Behavior of gravity deposited granular material under different stress paths. Can Geotech J 42(6):1644–1655
5. Sazzad MM, Suzuki K (2012) A comparison between conventional triaxial and plane-strain compression on a particulate system using 3D DEM. Acta Geotechnica Slovenica 9(2):17–23
6. Thornton C (2000) Numerical simulations of deviatoric shear deformation of granular media. Geotechnique 50(1):43–53
7. Ng T-T (2004) Macro- and micro-behaviors of granular materials under different sample preparation methods and stress paths. Int J solids Struct 41(21):5871–5884. https://doi.org/10.1016/j.ijsolstr.2004.05.050
8. Sazzad MM, Modaressi-Farahmand-Razavi SK, A, (2012) Macro-micro responses of granular materials under different b values using DEM. Int J Geomech 12(3):220–228. https://doi.org/10.1061/(ASCE)GM.1943-5622.0000133
9. Sazzad MM, Suzuki K (2013) Density dependent macro-micro behavior of granular materials in general triaxial loading for varying intermediate principal stress using DEM. Granular Matter 15(5):583–593. https://doi.org/10.1007/s10035-013-0422-z

10. Sazzad MM, Shaha RK, Islam MS, Kawsari S (2015) Macro and micro responses of granular materials under plane strain compression by 3D DEM. Int J Adv Structs Geotech Eng 4(2):114–119
11. Sazzad MM (2019) Effect of intermediate principal stress on the behavior of granular materials at a low mean stress by DEM. Geotech Geol Eng 37(5):4539–4550. https://doi.org/10.1007/s10706-019-00929-7
12. Cundall PA, Strack ODL (1979) A discrete numerical model for granular assemblies. Geotechnique 29(1):47–65. https://doi.org/10.1680/geot.1979.29.1.47
13. Kuhn MR (1999) Structured deformation in granular materials. Mech Mater 31(6):407–429. https://doi.org/10.1016/S0167-6636(99)00010-1
14. Kuhn MR (2003) Smooth convex three-dimensional particle for the discrete element method. J Eng Mech 129(5):539–547. https://doi.org/10.1061/(ASCE)0733-9399(2003)129:5(539)
15. Kuhn MR, Renken HE, Mixsell AD, Kramer SL (2014) Investigation of cyclic liquefaction with discrete element simulations. J. Geotech Geoenviron Eng 140(12):1–13. https://doi.org/10.1061/(ASCE)GT.1943-5606.0001181
16. Sazzad MM, Suzuki K (2010) Micromechanical behavior of granular materials with inherent anisotropy under cyclic loading using 2D DEM. Granular Matter 12(6):597–605. https://doi.org/10.1007/s10035-010-0200-0
17. Sazzad MM (2016) Micro-scale responses of granular materials at different confining pressures using DEM. Acta Geotech. Slovenica 13(1):26–36
18. Cornforth DH (1964) Some experiments on the influence of strain conditions on the strength of sand. Geotechnique 14(2):143–167
19. Satake M (1982) Fabric tensor in granular materials. In: Vermeer PA, Luger HJ (eds) Proceeding of IUTAM Symposium on Deform Fail of Granular Materials. Balkema, Delft, pp 63–68
20. Sazzad MM (2014) Micro-scale behavior of granular materials during cyclic loading. Particuology 16:132–141. https://doi.org/10.1016/j.partic.2013.12.005